약학석사학위논문

An Oncogenic Variant of AIMP2 Enhances K-Ras Stability *via* Heat Shock Protein Complex

발암성 변이체 AIMP2가 Heat Shock Protein Complex을 매개체로 하여 K-Ras를 안정화시켜 대장암을 유발시키는 과정에 대한 규명

2018년 01월

서울대학교 융합과학기술대학원
분자의학 및 바이오제약학과 의약생명과학전공

노 윤 아

An Oncogenic Variant of AIMP2 Enhances K-Ras Stability *via* Heat Shock Protein Complex

발암성 변이체 AIMP2가 Heat Shock Protein Complex을 매개체로 하여 K-Ras를 안정화시켜 대장암을 유발시키는 과정에 대한 규명

지도교수 김성훈

이 논문을 약학석사학위논문으로 제출함

2018 년 01 월

서울대학교 융합과학기술대학원
분자의학 및 바이오제약학과 의약생명과학전공
노 윤 아

노윤아의 석사학위논문을 인정함
2018 년 01 월

위 원 장 윤홍덕 (인)
부 위 원 장 신영기 (인)
위 원 김성훈 (인)

ABSTRACT

K-Ras is one of Ras small GTPase family and it facilitates diverse cell signaling. Many researches have shown that mutated K-Ras induces colorectal cancer. For last few decades, there have been intensive efforts to understand oncological implications of mutated K-Ras and to control its stability. However, these efforts fail to provide the amplification mechanisms of pathological level of K-Ras and also they could not provide clinically useful outcome to control the activity or expression level of K-Ras.

Here, I report the veiled mechanism of the pathological implication and stabilization of K-Ras. I propose AIMP2-DX2, as known as an exon2-deleted splicing variant of AIMP2 (aminoacyl-tRNA synthetase complex-interacting multifunctional protein 2), is the key factor regulating K-Ras. The GST domain of AIMP2-DX2 binds to the hypervariable region of K-Ras specifically. After AIMP2-DX2 and K-Ras interact each other, AIMP2-DX2 recruits the heat shock proteins, HSP70 and HSP90, to facilitated proper folding of K-Ras. This process enhances the stability and oncogenicity of K-Ras, which results the aggressive tumor progression. In the presence of both proteins, AIMP2-DX2 and K-Ras, the tumor progression is much more noticeable *in vitro*, *in vivo* conditions and tissue samples of colorectal cancer patients.

Therefore, I suggest that regulating the level of AIMP2-DX2 could be the one of the key factors to control the stability and oncogenicity of K-Ras. Through

this study, I believe that AIMP2-DX2-mediated novel mechanism of K-Ras is a strong therapeutic implication of colorectal cancer.

Key Words AIMP2-DX2, Colorectal Cancer, Hsp70, Hsp90, Heat Shock Protein Complex, K-Ras, Oncogenicity, Pathological implication, Therapeutic implication

Student Number 2016-26007

CONTENTS

LIST OF FIGURES and TABLES

ABBREVIATION LIST

AIMP2 : Aminoacyl tRNA Synthetase complex-interacting multifunctional Protein 2

AIMP2-DX2 : Aminoacyl tRNA Synthetase complex-interacting multifunctional Protein 2 whose Exon 2 is deleted (Exon 2 deletion mutant of AIMP2)

CRC : Colorectal Cancer

EV : Empty Vector

HSP : Heat Shock Protein

IHC : Immunohistochemistry

IP : Immunoprecipitation

MN : tumor and matched normal

NMR : Nuclear Magnetic Resonance

Q-PD : Quantitative *in vitro* pull down

Q-IP : Quantitative immunoprecipitation

S.D. : Standard Deviation

TMA : Tissue micro array

INTRODUCTION

Colorectal cancer (CRC) is a leading cause of cancer death worldwide (1). The development of CRC is a multiple stepwise process. It starts as normal colonic epithelial cells. Then, it turns into advanced adenoma and finally to carcinoma (1). Many reports have pointed out K-Ras as a significant factor in tumorigenesis of CRC. K-Ras has been detected as a mutated-form in about 30% of colorectal adenoma, and 30% to 50% of CRC (2). Surgery has been reliable method to treat the benign tumors. However, those who are in late stages of CRC, adjuvant therapies are the only reliable treatments. However, these therapies are known to have side effects, toxicity and tolerance (2). Therefore, novel therapy for CRC, which is based on better understanding of the molecular mechanisms of K-Ras, is needed to treat the CRC patients effectively.

Here, I report an oncogenic variant of AIMP2, AIMP2-DX2 (3), enhances the expression level and the oncogenecity of K-Ras. AIMP2 is one of nine ARSs (Aminoacyl tRNA synthetase), which composes MSC (multi-synthetase complex). Three AIMPs, AIMP1, 2, and 3, facilitate the assembly of MSC by interacting with each other and with their specific target enzymes (3, 4). In addition, AIMPs are known to involve in signaling pathways (5, 6). Especially, AIMP2 works as a potent tumor suppressor by promoting apoptosis through the protective interaction with p53 (7, 8). Moreover, AIMP2 mediates pro-apoptotic activity via interaction with FBP, TRAF2, and p53 under TGF-β, TNF-α, and genotoxic stress (9).

However, AIMP2-DX2, a splicing variant of AIMP2 lacking exon 2, blocks

the tumor suppressive activity of AIMP2 full length (AIMP2-F) by competitive binding to p53 (10). According to previous studies, the cells with higher level of AIMP2-DX2 have showed higher propensity to for anchorage-independent colonies and increased resistance to cell death (3, 9). Additionally, the patients with higher expression of AIMP2-DX2 showed lower survival and poor prognosis. Therefore, suppression of AIMP2-DX2 has been considered as a new therapeutic target to slow down the tumor growth (15).

In addition, the expression of AIMP2-DX2 resulted the synergistic effect of tumorigenesis in K-Ras-driven mouse (10). However, the functional relationship of the two oncoproteins was not understood. Through this research, I have found that oncogenic AIMP2-DX2 enhances the expression level of K-Ras. As the expression level of AIMP2-DX2 increases, the expression level of K-Ras is also increased. However, K-Ras binding-defective AIMP2-DX2 mutants fail to increase the expression level of K-Ras. Also, in vivo analysis using with and without K-Ras binding-defective AIMP2-DX2 mutants, I obtained same result as above.

Moreover, AIMP2-DX2 seems to have ability to recruit heat shock protein complex, HSP70 and HSP90, to stabilize the K-Ras. First, AIMP2-DX2 binds to K-Ras and then HSP 70 is recruited to the binding site. For further proper folding of K-Ras, HSP90 is recruited and binds with K-Ras, which results oncogenic characteristic of K-Ras. Through this process, K-Ras also obtains the tumoregenesis. As a result, AIMP2-DX2 facilitates the proliferation and transformation of K-Ras and AIMP2-DX2 is the significant factor to generate the CRC.

This work unveiled a previously unidentified interaction of two oncogenic proteins, AIMP2-DX2 and K-Ras, and suggests the pathological therapeutic implications. I suggest that the AIMP2-DX2 is a strong candidate target to cure CRC. If the interaction of AIMP2-DX2 and K-Ras can be inhibited, then the oncogenetic progress of K-Ras can be controlled.

MATERIALS AND METHODS

Anchorage-independent colony formation assay

HCT-116 cells (5×10^5) expressing GFP-K-Ras and Strep-AIMP2-DX2 were subjected to anchorage-independent colony formation assay by using cell transformation assay kit (CELL BIOLABS, INC.), following the manufacturer's instruction. After 10 days, settled colonies were stained with MTT solution (Sigma) and the numbers of colonies were counted. The experiments were repeated three times independently.

Cell culture and materials

COLO-205, HCT-8, KM-12, SNU-C4, SW-403, NCI-H747 and SNU-407 cell lines were purchased from Korea Cell Line Bank. CCD18CO, HCT-116, DLD-1, LoVo, WI-26 and H460 cell lines were obtained from BioBank of Biocon. CCD18CO and WI-26 cells were cultured in DMEM and other cell lines in RPMI supplemented with 10% FBS and 1% penicillin/streptomycin in 5% CO_2 at 37 ℃. All the plasmids for GFP-tagged Ras proteins are kind gifts from Dr. Mark R. Philips and sub-cloned at *Eco*RI/*Xho*I sites of pNL1.1 vector (Promega). Human AIMP2-DX2 was cloned at *Eco*RI/*Xho*I sites of pEXPR-IBA5 vector. Point mutagenesis of AIMP2-DX2 and Ras was performed using Quik-ChangeII (Promega), following the manufacturer's instruction. Doxycycline and puromycin were purchased from Peprotech and Sigma, respectively. Specific antibodies against AIMP2-F and

AIMP2-DX2 were purchased from Neomics. FLAG and Strep antibodies were bought from Sigma and IBA, respectively.

Generation of inducible AIMP2-DX2 knock-in mouse and embryonic fibroblast cells

To generate inducible human AIMP2-DX2 transgenic mouse, the tetO-AIMP2-DX2 construct was prepared under the control of a minimal promoter from hCMV fused to the tetO sequence. This construct was subcloned into ROSA targeting vector (Soriano P's lab). The targeting vector was electroporated into mouse ES cells (E14TG2a), according to a previously reported procedure (7). Correctly targeted clones were screened by southern analysis and were injected into C57BL/6 blastocysts for chimera generation. Germline transmission of transgene allele was verified by PCR. Pups with human AIMP2-DX2 transgene were genotyped using the primer for the ROSA locus and maintained in homozygous colony ($ROSA^{hAIMP2\text{-}DX2/hAIMP2\text{-}DX2}$). CAG-rtTA3 transgenic mice (016532, The Jackson Laboratory) were crossed with hAIMP2-DX2 transgenic to generate doxycycline-inducible hAIMP2-DX2 mouse colony (CAG-rtTA3; $ROSA^{hAIMP2\text{-}DX2/+}$). Doxycycline diet (TD.01306, Harlan Teklad) was given to the mice *ad libitum* for 1 month for the sufficient induction of human AIMP2-DX2. Primers for ROSA locus as following: ROSA1, AAAGTCGCTCTGAGTTGTTAT; ROSA2: GGCGGGCCATTTACCGTAAG; ROSA3: GGAGCGGGAGAAATGGATATG. Mouse embryonic fibroblast (MEF) cells were prepared at embryonic day 13 from the cross between CAG-rtTA3 and

hAIMP2-DX2 transgenic mouse. Doxycycline-inducible MEFs were selected by genotyping and used for further experiments. Doxycycline (1 μg/ml) was added to the culture medium for hAIMP2-DX2 induction.

Immunohistochemistry

TMA slides (US Biomax, Inc.) were deparaffinized and then rehydrated in different percentages of ethanol (100, 95, 80 and 70%). Endogenous peroxidases were removed with 0.3% H_2O_2 (Sigma-Aldrich, St. Louis, USA) in PBS for 10 min and then antigen retrieval was performed using 10 mM citric buffer (pH 6.0) at 95 ℃ for 5 min. The TMA slides were blocked with 4% BSA in PBS for 30 min, incubated with primary antibodies at 4 ℃ for 12 hours and washed with PBS 3 times. Anti-rabbit/mouse-HRP (Dako, Carpinteria, USA) was then applied for 1 hr. The slides were developed with DAB and Chromogen mixture (Dako, Carpinteria, USA). A nuclear counter staining was carried out with Mayer's haematoxylin (Sigma-Aldrich, St. Louis, USA). The TMA slides were dehydrated in different percentages of ethanol (70, 80, 90 and 100%), cleared in xylene and then mounted. The level of stained-protein intensity was scored as 0 (<5% positive), 1 (5-40% positive), 2 (>40% positive). The numerical score was validated by a second independent examination. Primary antibodies against K-Ras and AIMP2-DX2 were purchased from Novusbio and Neomics, respectively.

Interactome analysis

Same amounts of lysates from GFP-EV- and -K-Ras-expressing 293T cells were reduced with 10 mM DTT for 30 min at 37 ℃ and alkylated with 40 mM iodoacetamide for 1hr in the dark at 25 ℃. The samples diluted 10-fold with 50 mM NH_4HCO_3 were treated with trypsin/Lys-C (Promega) at a ratio of 1:40 (w:w), followed by incubation overnight at 37 ℃. After purification of tryptic peptide by C_{18} spin column, purified peptide were dried and subjected to analysis on a LTQ-Orbitrap Velos (Thermo Fisher Scientific) connected to Easy-nano LC II system (Thermo Fisher Scientific) incorporating an autosampler. The dried peptides were resuspended in 0.1% formic acid, and one-tenth was injected to a reversed-phase peptide trap EASY-Column (L 2 cm, ID 100 μm, 5 μm, 120 Å, ReproSil-Pur C_{18}-AQ, Thermo Fisher Scientific) and a reversed-phase analytical EASY-Column (L 10 cm, ID 75 μm, 3 μm, 120 Å, ReproSil-Pur C_{18}-AQ, Thermo Fisher Scientific), and electrospray ionization was subsequently performed using a 30 μm nano-bore stainless steel online emitter (Thermo Fisher Scientific). The duration of total LC gradient was 120 min. The peptides were eluted in a linear gradient of 10 ~ 40% buffer B over 98 min with buffer A (0.1% formic acid in H_2O) and buffer B (0.1% formic acid in acetonitrile) and a flow rate of 300 nl/min. The LTQ-Orbitrap Velos mass analyzer was operated in positive ESI mode using collision-induced dissociation (CID) to fragment the HPLC separated peptides. The temperature and voltage applied to the capillary was 275 ℃ and 1.9 V. All data were acquired with mass spectrometer operating in automatic data-dependent switching mode. The MS

survey was scanned from 350 to 2000 m/z with resolution set to 100,000. The automatic gain control (AGC) target set to 1,000,000 ions with a maximum fill time of 500 ms. The 20 data-dependent MS/MS scans were selected and fragmented in the ion trap using an isolation window of 2.0 *m/z*, an AGC target value of 10,000 ions, a maximum fill time of 100 ms, a normalized collision energy of 35 and activation time of 10 ms. Dynamic exclusion was performed with a repeat count of 1, exclusion duration of 180 s, and a dynamic exclusion list size 500. A minimum MS ion count for triggering MS/MS set to 5000 counts. Each sample was subjected to a total of 3 LC-MS/MS runs (triplicated runs per sample). All MS/MS samples were analyzed using Sequest (XCorr Only) (Thermo Fisher Scientific, San Jose, CA, USA; version v.27, rev.11) and X! Tandem (The GPM, thegpm.org; version CYCLONE (2010.12.01.1)) using human database (Uniprot human, release 2014) containing 162,717 entries. Search parameters were set as following. The precursor mass tolerance of 25 ppm, fragment mass tolerance of 1.0 Da, and maximum missed cleavage of 2 were set. Carbamidomethylation (+57.021 Da) of cysteine (C) was set in Sequest (XCorr Only) and X! Tandem as a fixed modification. Oxidation (+15.995 Da) of methionine (M) was set in Sequest (XCorr Only) and X! Tandem as variable modifications. Scaffold searched the additional variable modifications: Glu→pyro-Glu (-18.01), Ammonia-loss (-17.03), and Gln→pyro-Glu (-17.03). Each processed data was subsequently transformed to *.sf file with Scaffold 4 Q+S program (version 4.6.1, Proteome Software Inc., Portland, OR). Scaffold program was used to validate MS/MS based peptide and protein identifications and to

process the quantitative analysis. Peptide identifications were accepted if they could be established at greater than 90.0% probability by the Peptide Prophet algorithm (11) with Scaffold delta-mass correction. Protein identifications were accepted if they could be established at greater than 90.0% probability and contained at least 1 identified peptides. Protein probabilities were assigned by Protein Prophet algorithm (12). Proteins that contained similar peptides and could not be differentiated based on MS/MS analysis alone were grouped to satisfy the principles of parsimony. The 'Total Ion Count (TIC)' (quantitative analysis method in the scaffold software) was used to calculate the fold change of individual proteins in samples.

In vivo analysis

H460 stable cells (2×10^7) expressing sh-AIMP2-DX2 and GFP-K-Ras4B^{G12C}, and HCT-116 stable cells (1×10^7) expressing GFP-K-Ras4B^{G12D} and Strep-AIMP2-DX2 were subcutaneously injected into two sites (left / right) of the back of 7-week-old female BALB/cAnCr mice (n = 4 / group). After three days of injection, tumor sizes and body weights were measured for the fifteen (H460) and seventeen days (HCT-116). After experimental day, all the mice were sacrificed and the embedded tumors were isolated. The size and weight of each isolated tumor were measured. Animal experiments were in compliance with the University Animal Care and Use Committee guidelines at Seoul National University.

MTT

The cells (1×10^4) were seeded in 96-well plates and cultured for 24 hrs. 10 μl of MTT solution (5 mg/ml, Sigma) was added to each well containing 100 μl medium and incubated for 30 min at 37 ℃. The precipitated formazan crystals were dissolved in 100 μl DMSO (Duchefa). Absorbance was measured at 420 nm using a microplate reader (Sunrise, TECAN).

NMR analysis

^{15}N-labeled AIMP2-DX2$_{51-251}$(C136S, C222S) was overexpressed and purified from *E. coli*, strain BL21-CodonPlus(DE3)-RIPL in M9 minimal medium enriched with $^{15}NH_4Cl$ as the sole nitrogen source (99% ^{15}N; Cambridge Isotope Laboratories) [20]. The ^{1}H-^{15}N TROSY experiments were performed with 0.3 mM ^{15}N-labeled AIMP2-DX2$_{51-251}$(C136S, C222S) in the presence and absence of 3.0 mM K-Ras4A$_{169-195}$ in buffer 20 mM Bis-Tris (pH 6.0), 100 mM NaCl, 100 mM glycin, 1 mM dithiothreitol (DTT) and 1 mM phenylmethylsulfonyl fluoride (PMSF) at 298 K. To avoid pH changes upon the addition of the peptide, we conducted dialysis in a same beaker, using a membrane with 500 dalton cut off, for both samples with and without the peptide, respectively. The backbone assignment of ^{13}C, ^{15}N-labeled AIMP2-DX2$_{51-251}$(with the substitutions of C136S and C222S) was performed with series of triple-resonance two- and three-dimensional experiments. Data were processed with NMRpipe (8) and analyzed with CCPN2.1.5 (9). CSP of ^{15}N and ^{1}H nuclei were analyzed by overlaying the ^{1}H-^{15}N TROSY

spectra of free protein with those with K-Ras4A$_{169-195}$. The magnitude of the combined ^{1}H-^{15}N chemical shift differences (Δδ, ppm) was calculated using the equation $\Delta\delta = [0.5 \times (\delta H^2) + 0.2 \times (\delta N^2)]^{1/2}$, where δH and δN are changes to the proton (^{1}H) and nitrogen (^{15}N) chemical shifts, respectively (10). All the NMR spectra were recorded using an Avance 600 MHz NMR spectrometer equipped with a triple-resonance probe (Bruker, Germany).

Patient analysis

Tumor and matched normal tissues of colorectal cancer patients were obtained from Yonsei hospital. All the tissues (n = 99) were lysed with 50 mM Tris-HCl (pH 7.4) buffer containing 100 mM NaCl, 0.5% Triton X-100, 0.1% SDS, 10% glycerol, 1 mM EDTA, and protease inhibitor (Calbiochem). The lysates were subjected to SDS-PAGE and Western blotting using the specific antibodies against AIMP2-DX2, K-Ras and actin. The levels of AIMP2-DX2 and K-Ras were quantified and normalized by those of actin. The normalized values in tumors and paired normal tissues were compared.

Quantitative co-immunoprecipitation

Nanoluciferse-tagged Ras and Strep-AIMP2-DX2 were introduced into CCD18CO cells. The cells were lysed with 50 mM Tris-HCl (pH 7.4) buffer containing 100 mM NaCl, 0.5% Triton X-100, 0.1% SDS, 10% glycerol, 1 mM EDTA, and protease inhibitor (Calbiochem) and centrifuged. The supernatants were precipitated

with Strep-Tactin Sepharose Column (IBA), following the manufacturer's instruction. The luciferase activities of elute were normalized by those of whole cell lysates after excluding the background luciferase activities of the control in which Strep-AIMP2-DX2 was not expressed. The luciferase activity was measured by using nanoluciferase assay system, following the manufacturer's protocol (Promega). The experiments were repeated three times independently.

Quantitative *in vitro* pull down assay

GST-tagged proteins were incubated with nanoluciferase-tagged Ras-expressing 293T cell extracts in 50 mM Tris-HCl (pH 7.4) binding buffer containing 100 mM NaCl, 0.5% Triton X-100, 10% glycerol, 1 mM EDTA, and protease inhibitor (Calbiochem). After incubation for 4 hrs at 4 ℃, GST-proteins were precipitated with glutathione-sepharose beads and washed with binding buffer three times. The amounts of co-precipitates with GST-proteins were measured by the luciferase activity (Promega). Those of the extracts normalized the activities after removing the background activity bound to GST-EV. The experiments were repeated three times independently.

RESULTS

AIMP2-DX2 specifically stabilizes K-Ras via binding

To check how the induction of AIMP2-DX2 would affect K-Ras level, I generated transgenic mouse in which AIMP2-DX2 expression level has been induced by treatment of doxycycline (Dox). And then, colon tissues, the expression levels of AIMP2-DX2 were induced, were analyzed. For its control, colon tissues from normal mice were prepared. After analyze the level of K-Ras from each group, it was clear to conclude that the level of K-Ras was significantly increased by the induction of AIMP2-DX2 (Fig. 1a). I also prepared AIMP2-DX2-inducible mouse embryonic fibroblasts and examined the effect of AIMP2-DX2 on K-Ras level. As the Dox-dependent induction of AIMP2-DX2 increased, K-Ras level was increased also (Fig. 1b). To determine whether AIMP2-DX2 binds to K-Ras specifically, we incubated the purified GST-AIMP2-DX2 with different Ras proteins. Through *in vitro* pull-down assay, AIMP2-DX2 interacted with K-Ras but not N- or H-Ras (Fig. 1c). And then, to figure out the exact domain sites of two proteins that are responsible for the binding, AIMP2-DX2 was divided into N-terminal domains (DM1) and GST domains (DM2), and K-Ras was divided into G-domain and hypervariable region (HVR)-domains (Fig. 1d) (13, 14). Using Co-immunoprecipitation and *in vitro* pull down assays, the GST domain of AIMP2-DX2 binds to HVR domain of K-Ras when two proteins interact each other (Fig. 1e and f). The reason why AIMP2-DX2 specifically interacts to K-Ras is because the

HVR regions of three Ras isoforms contain their own distinctive amino acid residues (Fig. 1g) (3, 13). Since K-Ras has more lysine residues than N- or H-Ras, K-Ras only can interact with AIMP2-DX2 because K-Ras is more positive charged than N- or H-Ras.

Threonine 85 and Lysine 90 of AIMP2-DX2 are critical for binding with K-Ras

To understand the interaction of the two proteins in detail, I performed the NMR-based chemical shift perturbation (CSP) analysis using ^{15}N-labeled AIMP2-DX2$_{51-251}$ (with C136S and C222S substitutions) (15) in the presence and the absence of K-Ras HVR peptide. In NMR analysis, His84, Thr85, Lys90 and Trp120 residues showed strong perturbation while Leu64 and Val83 were weakly perturbed (Fig. 2a). The K-Ras HVR binding residues were linearly aligned along with the hydrophobic cleft formed between alpha helix bundle and β-sheet of the GST domain of AIMP2-DX2 (Fig. 2b). To validate the NMR results, I generated alanine substitution AIMP2-DX2 mutants that could interrupt the interaction with K-Ras. And these K-Ras-binding defective AIMP2-DX2 mutants were produced based on the NMR analysis and examined the mutational effects on the interaction. Quantitative *in vitro* pull down (Q-PD) and immunoprecipitation (Q-IP) assays showed that alanine substitutions at Thr85, Lys90 and Val92 reduced the binding interaction with K-Ras (Fig. 2c, 2d). Moreover, relative K-Ras level was reduced when then mutation of Thr85, Lys90 and Val92 were introduced (Fig. 2e). Thr85,

Lys90 and Val92 of AIMP2-DX2 form a pocket responsible for binding with HVR peptide of K-Ras. Val92 appears to be positioned in slight sideways from binding pocket, explaining why its mutation would be less influential than Thr85 and Lys90 (Fig. 2f).

Interactome analysis of K-Ras

Not only AIMP2-DX2, but also K-Ras are not known to have protein-folding function. Therefore, to understand how AIMP2-DX2 would stabilize K-Ras, I expressed GFP-K-Ras in 293T cells and the binding proteins were determined by LC-MS analysis after co-immunoprecipitation. Among 145 identified proteins, 31 proteins were specifically bind to K-Ras (Fig. 3a). Based on Ontology classification, two components of heat shock proteins were related to K-Ras (16) (Fig. 3b). Moreover, HSPA1L (heat shock protein 70kDa 1L) peptide was most frequently detected (Fig. 2c). To validate the relationship between K-Ras and heat shock protein, I further checked the binding of endogenous heat shock proteins and K-Ras. GFP-K-Ras was co-immunoprecipitated wish HSP70, HPS90 and HSP40. HSP40 appeared to bind less strongly compared to HSP70 and HSP90 (Fig. 2d). These results imply how AIMP2-DX2 stabilizes the K-Ras. Since AIMP2-DX2 or K-Ras do not have protein-folding capability, heat shock proteins are recruited to further proper folding of K-Ras.

AIMP2-DX2 recruits the heat shock protein complex, HSP70 and HSP90, to K-Ras for further folding

I performed co-immunoprecipitation of both HSP70 and HSP90 with K-Ras at different levels of AIMP2-DX2. Binding of heat shock protein complex, HSP70 and HSP90, to K-Ras showed strong dependency on the expression levels of AIMP2-DX2 (Fig. 4a). This was also confirmed by *in vitro* pull-down assays (Fig. 4b). Moreover, the positive effect of HSP70 and HSP90 on K-Ras level was more apparent in the presence of high level of endogenous AIMP2-DX2 (Fig. 4c). The K-Ras-binding defective AIMP2-DX2 mutants could not induce the association of K-Ras and heat shock protein complex; HSP70 and HSP90 (Fig. 4d). Within these results, Hsp70 and Hsp90 critical factors to stabilize the K-Ras, and heat shock protein complex can fold the K-Ras properly only in the presence of AIMP2-DX2.

Determination of the domains of K-Ras, HSP70 and HSP90 that involved in the binding interaction

To understand detailed binding sites of K-Ras with HSP70 and HSP90, I determined the domains responsible for their interactions by *in vitro* pull down assays and immunoprecipitation. The results showed the G-domain of K-Ras binds to substrate binding domain (SBD) of HSP70, and G-domain of K-Ras binds to middle (MD) and C-terminal domain (CTD) of HSP90 (Fig. 5b-e). The SBD of HSP70 and MD and CTD of Hsp90 are known as the client recognition domains

(17). Therefore, this implies that K-Ras is one of substrates of Hsp70 and Hsp90, and K-Ras is stabilized by common mechanism of chaperone complex. Altogether, I concluded that AIMP2-DX2 would trigger sequential recruitment of HSP70 and HSP90 to K-Ras for proper folding and stability of K-Ras.

AIMP2-DX2 enhances the oncogenicity of K-Ras

AIMP2-DX2 enhances the expression level and stability of K-Ras by recruiting heat shock protein complex. Then, I wondered whether AIMP2-DX2 would affect the oncogenic activity of K-Ras. First, I analyzed oncogenic significance of AIMP2-DX2 and K-Ras using anchorage-independent colony forming and cell proliferation assays. While AIMP2-DX2 wild type (WT) enhanced colony formation and cell proliferation activities by regulating K-Ras, the K-Ras binding-defective T85A and K90A mutants of AIMP2-DX2 did not show oncogenic activities (Fig. 6b). And then, I generated H460 cell lines in which contain over-expressed level of the K-Ras4B^{G12C} mutant in order to check the tumor progression. Each cell line was subcutaneously xenografted into the back of mouse and tumor growth was analyzed for 17 days. Only when AIMP2-DX2 WT is introduced to these cells, the tumor progression was faster and the tumor size was largest. However, the K-Ras binding-defective AIMP2-DX2 mutants couldn't enhance the oncogenecity of K-Ras (Fig. 6c-f). All of these results suggest that AIMP2-DX2 but only induces the expression level of K-Ras, but also promotes the oncogenicity of K-Ras.

Positive correlation of AIMP2-DX2 and K-Ras in colon cancer

To see clinical relevance of the interaction of AIMP2-DX2 and K-Ras, I analyzed the expression levels of AIMP2-DX2 and K-Ras in colorectal cancer cell lines in which K-Ras mutations are frequently found (14, 18). Among 11 colorectal cell lines, SW-403, NCI-H747, SNU-407, DLD-1 and LoVo showed the high cellular expression level of AIMP2-DX2 and K-Ras. Others, CCD18C0, COLO-205, HCT-116, HCT-8, KM-12, and SNU-C4 showed both low expression level of AIMP2-DX2 and K-Ras. Analysis of colorectal cell lines concluded that these two proteins, AIMP2-DX2 and K-Ras, are positively correlated to each other (Fig. 7a). Also, the tissues of colorectal cancer patients were analyzed using immunohistochemistry (IHC) staining. Based on the staining intensity, 62% of colon cancer samples (n = 31/50) showed high levels of AIMP2-DX2 and K-Ras simultaneously (Fig. 7b). In addition, 18% of colon cancer tissues showed low levels of both proteins. For more refined analysis, I obtained matched tumor and normal tissues from colon cancer patients (n = 99) and analyzed the tissue levels of the two proteins by immunoblotting (Fig. 7c). In this case, 30% (n = 30/99) of samples showed high expression levels of both proteins, and 44% (n = 43/99) of samples showed low levels of both proteins. These results support the tight association of AIMP2-DX2 and K-Ras and their relationship causes the tumor progression in human tissue.

LIST OF FIGURES and TABLES

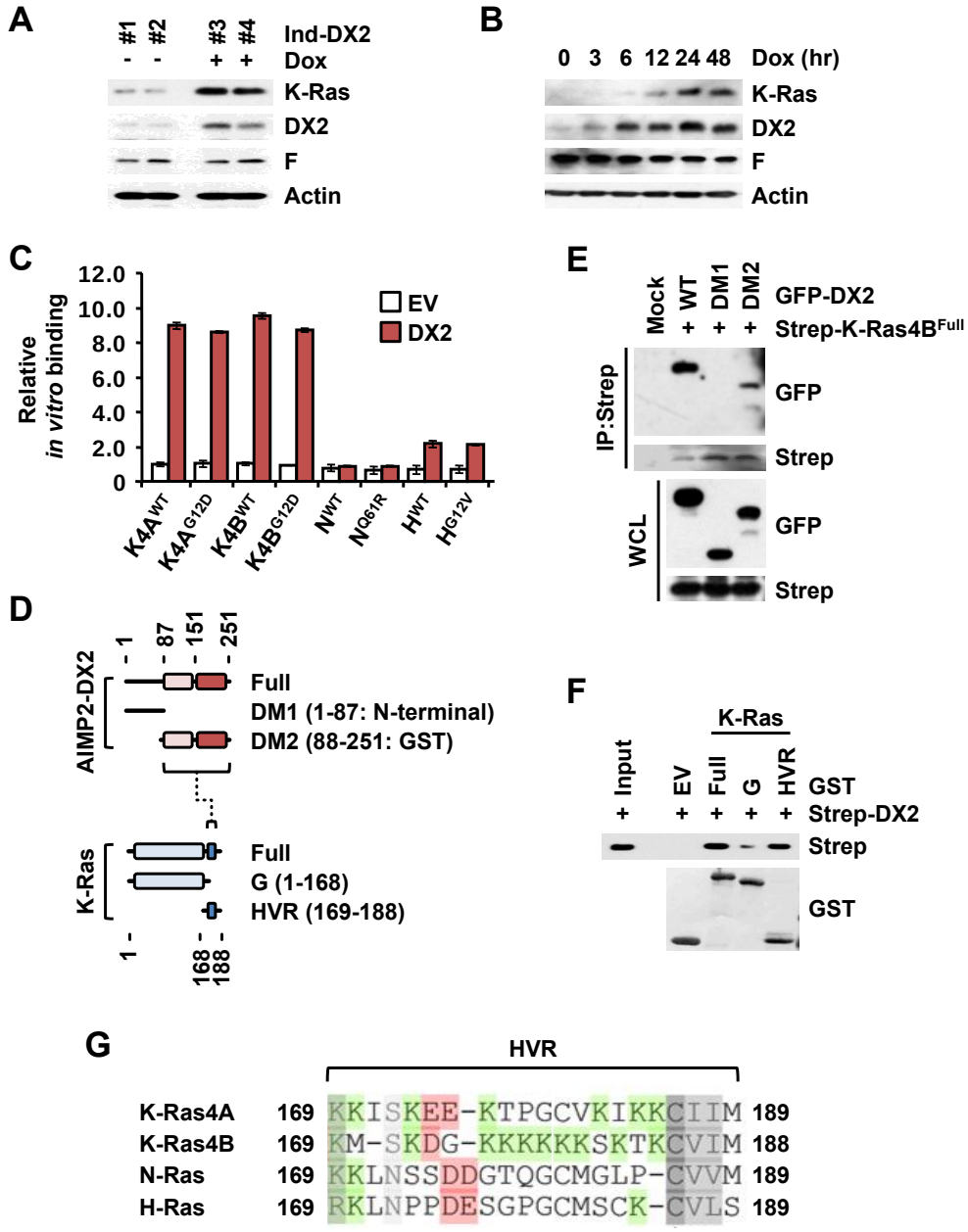

Figure 1. AIMP2-DX2 specifically stabilizes K-Ras via binding

(A) Doxycycline (Dox)-inducible AIMP2-DX2 transgenic mice were fed with doxycycline-containing food. After 17 days later, colons were isolated from two normal mice (#1, 2) and two Dox-fed mice (#3, 4). And then, the levels of K-Ras and AIMP2-DX2 were determined by Western blotting.

(B) Mouse embryonic fibroblasts (MEF) cells were isolated from AIMP2-DX2-inducible transgenic mice. After these cells were treated with Dox, the level of K-Ras and AIMP2-DX2 were determined by Western blotting at time interval.

(C) Strep-AIMP2-DX2 was introduced into CCD18CO cells after expressing wild type of GFP-K-Ras, GFP-H-Kras and GFP-N-Ras and their mutants. Cell growth was measured by MTT assay and represented as a bar graph. The experiments were repeated three times and error bar means S.D.

(D) Arrangement of functional domains present in AIMP2-DX2 and K-Ras. Binding regions of the two proteins is marked with brackets.

(E) Each different domains of AIMP2-DX2 (DM1 and DM2) fused to GFP and Strep-K-Ras4B full-length were co-expressed in 293T cells. And, they were precipitated using Strep-tag column. Co-precipitated domain of AIMP2-DX2 was determined by Western blotting with anti-GFP antibody.

(F) Strep-AIMP2-DX2 was incubated with different domains of K-Ras (Full, G, and HVR) fused to GST. After precipitation with glutathione-sepharose

beads, co-precipitation with AIMP2-DX2 was determined by Western blotting with anti-Strep antibody. Expressions of GST proteins were confirmed by coomassie staining.

(G) Amino acid sequence alignment of K-Ras4A, K-Ras4B, N-Ras and H-Ras is represented as a picture. Grey, green, and pink color indicates the similarity, positive charge and negative charge, respectively.

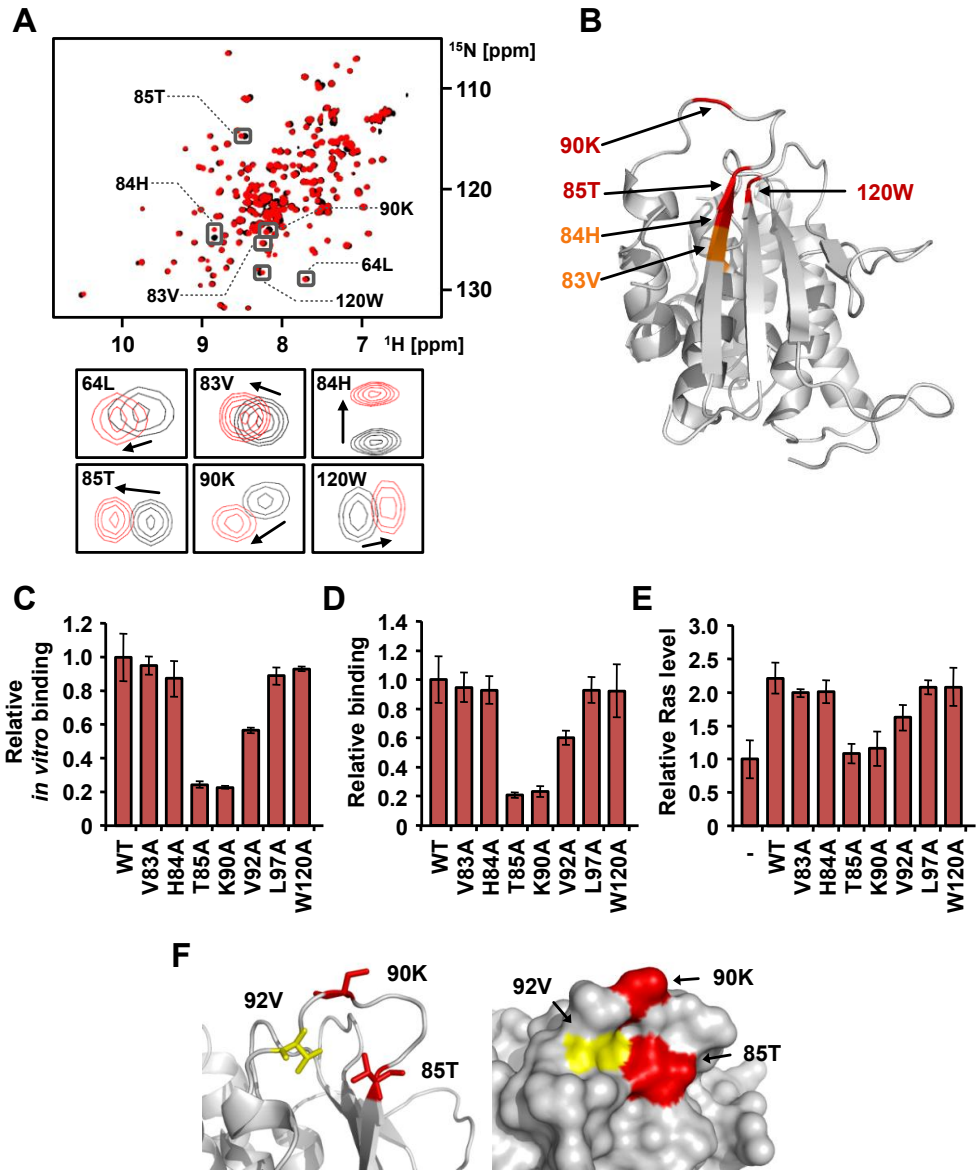
A
15N [ppm]
110
120
130
85T
84H
90K
64L
83V
120W
10
9
8
7
1H [ppm]
64L
83V
84H
85T
90K
120W
B
90K
85T
84H
83V
120W
C
Relative in vitro binding
1.2
1.0
0.8
0.6
0.4
0.2
0
WT
V83A
H84A
T85A
K90A
V92A
L97A
W120A
D
Relative binding
1.4
1.2
1.0
0.8
0.6
0.4
0.2
0
WT
V83A
H84A
T85A
K90A
V92A
L97A
W120A
E
Relative Ras level
3.0
2.5
2.0
1.5
1.0
0.5
0
-
WT
V83A
H84A
T85A
K90A
V92A
L97A
W120A
F
90K
92V
85T
92V
90K
85T

Figure 2. Threonine 85 and Lysine 90 of AIMP2-DX2 are critical for binding with K-Ras

(A) CSP of ^{15}N-labeled AIMP2-DX2$_{51-251}$(C136S, C222S) by the binding to K-Ras4A$_{169-195}$, HVR peptide. Superposition of the 2-dimensional (2D) ^{1}H-^{15}N TROSY spectra of free 0.3 mM AIMP2-DX2$_{51-251}$(C136S, C222S) in the presence (red) and absence (black) of 3.0 mM HVR peptide. Strongly perturbed residues are presented in rectangular box (bottom).

(B) Strongly ($\Delta\delta > 0.02$ ppm) and mildly ($0.01 < CSP \leq 0.02$ ppm) perturbed residues are shown in red and orange, respectively, on the surface of AIMP2-DX2 (Left). The weighted average of chemical shift changes, $\Delta\delta$, was calculated by the equation $\Delta\delta$ (ppm) = $[0.5 \times ((\delta H)^2 + 0.2 \times (\delta N)^2)]^{1/2}$. Model for binding of the K-Ras HVR domain to AIMP2-DX2 GST domain, AIMP2-DX2$_{51-251}$. HVR domain of K-Ras was denoted as light-green dashed line. The strongly and mildly perturbed residues of AIMP2-DX2 by the binding were shown as red and orange colors on the surface of AIMP2-DX2, respectively (Middle). The surface electrostatic potential of the GST domain of AIMP2-DX2 was presented with the same orientation (Right).

(C) Nanoluciferase-tagged AIMP2-DX2 mutants were mixed with purified GST-K-Ras4B and precipitated with glutathione-sepharose beads. The amounts of co-precipitated AIMP2-DX2 mutants were quantitatively measured the luciferase activity. The results were represented as a bar graph.

(D) Strep-AIMP2-DX2 mutants were introduced into DDC18CO cells expressing nanoluciferase-K-Ras and precipitated by Strep-tag column. The amounts of co-precipitated K-Ras were measured by the luciferase activity.

(E) The lysate of the same cell from figure D were subjected to the luciferase assay to determine K-Ras level.

(F) The residues of AIMP2-DX2 critical for the binding to K-Ras are highlighted. Strongly (85T and 90K) and weakly (92V) affecting residues are colored by red and yellow, respectively.

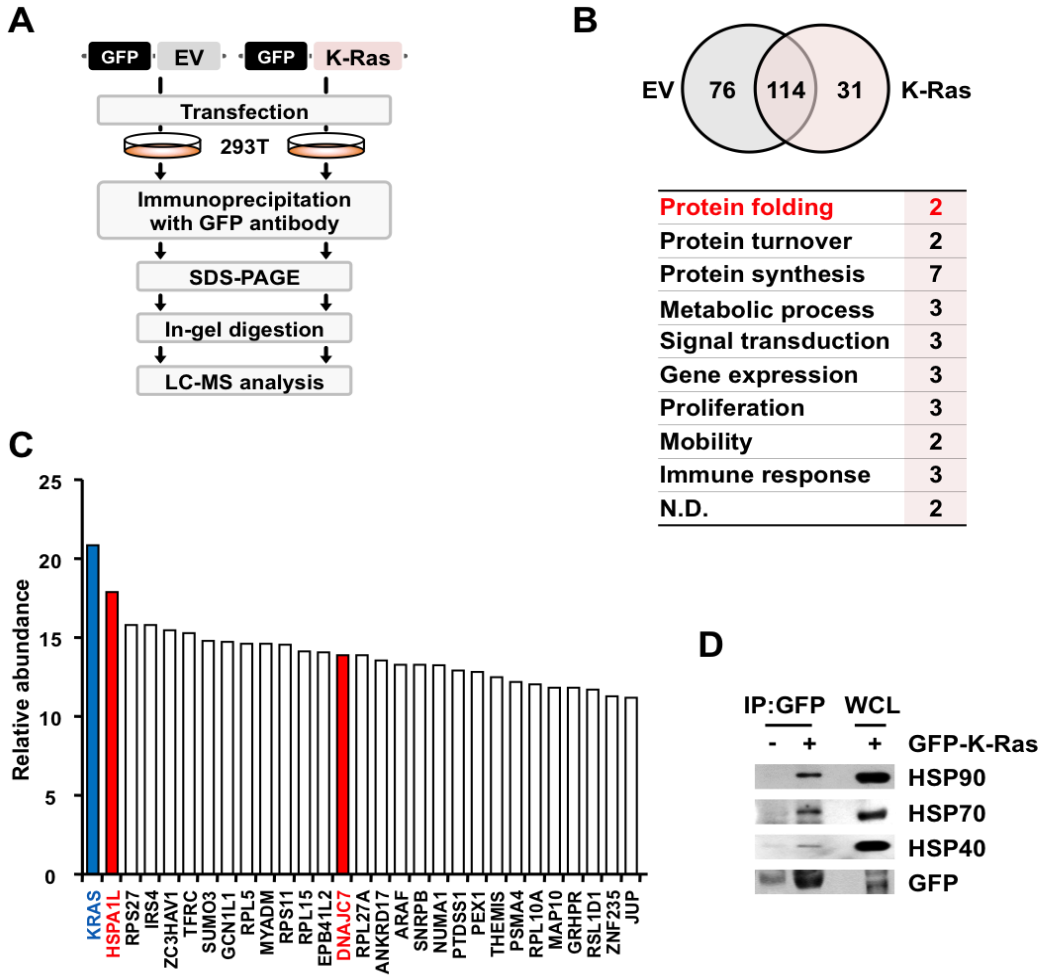

Figure 3. Interactome analysis of K-Ras

(A) Flow chart of proteomic AP-MS for determining K-Ras interactome.

(B) Venn Diagram showing the protein numbers co-precipitated with GFP and GFP-K-Ras. EV means empty vector. The table represents the functional classification of K-Ras interactome.

(C) Relative abundance of unique proteins that were identified as K-Ras-

binding proteins. The horizontal axis indicates the name of interacting protein and the vertical axis indicates the relative abundance compared with EV. Blue bar represents the K-Ras as a bait and red bar indicates the heat shock proteins.

(D) GFP-K-Ras expressed in 293T cells were immunoprecipitated with anti-GFP antibody and co-precipitation of HSP90, HSP70 and HSP40 was determined by Western blotting with their specific antibodies.

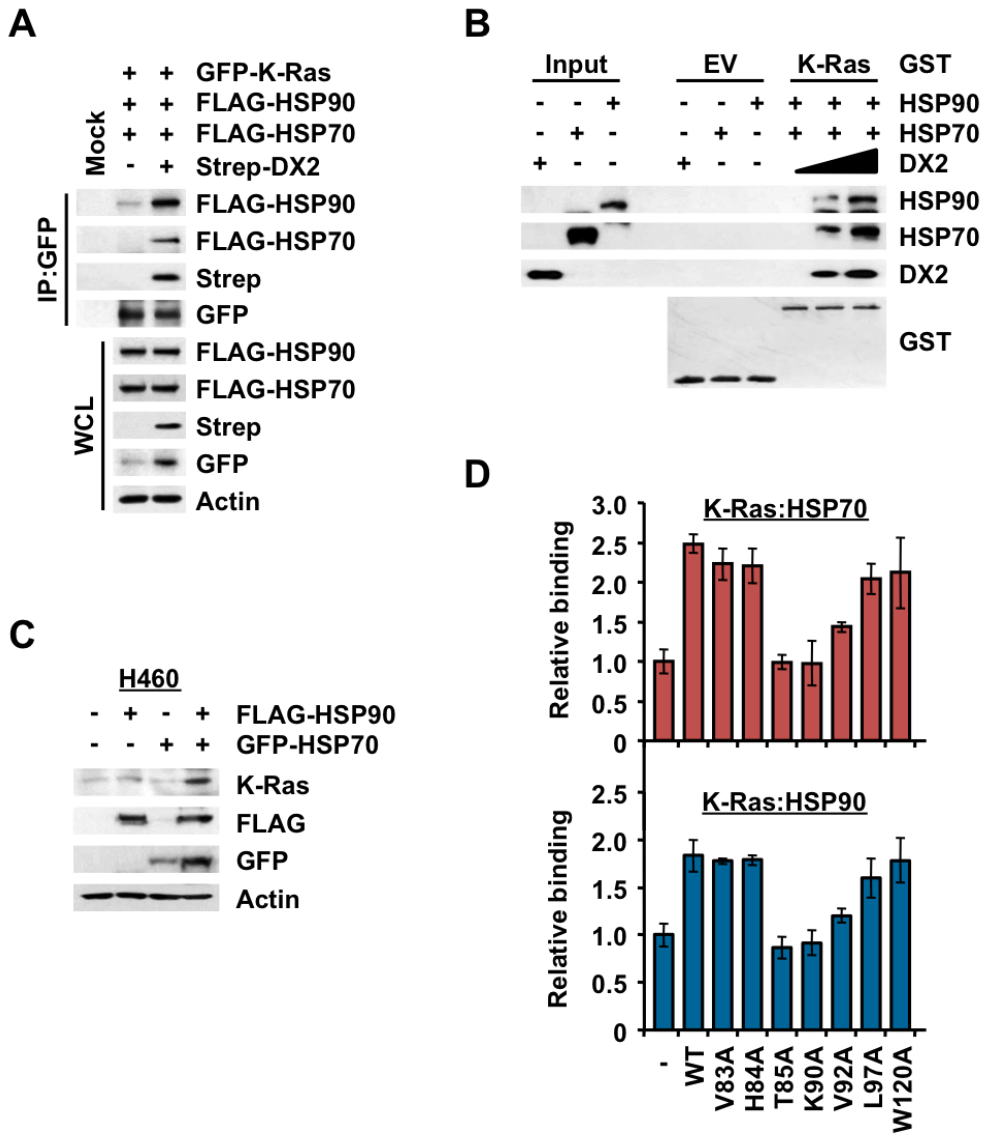

Figure 4. AIMP2-DX2 recruits the chaperone complex, HSP70 and HSP90, to K-Ras

(A) AIMP2-DX2 was up-regulated by introducing Strep-AIMP2-DX2 to 293T

cells. And then, GFP-K-Ras, FLAG-HSP90 and FLAG-HSP70 were expressed in these cells. GFP-K-Ras was immunoprecipitated with anti-GFP antibody and co-precipitation of other proteins were determined by Western blotting with their respective antibodies.

(B) HSP70 and HSP90 in the cell lysates were incubated with the purified GST-K-Ras proteins in the presence of up-regulated the level of AIMP2-DX2. After precipitated with glutathione-sepharose beads, co-precipitation of HSP70 and HSP90 was determined by Western blotting with their specific antibodies. Then, GST proteins were detected by coomassie staining.

(C) Effects of FLAG-HSP90 and GFP-HSP70 on a cellular level of K-Ras were determined by Western blotting in H460 cells.

(D) Each of FLG-HSP70 (upper) and FLAG-HSP90 (bottom) was introduced into CCD18CO cells. These CCD18CO cells were already transfected with nanoluciferase-K-Ras and AIMP2-DX2 (wild type and mutants). K-Ras defective binding mutants of AIMP2-DX2 affected on the binding of each HSP70 and HSP90 to K-Ras. This result was monitored by the luciferase activity of nanoluciferase-K-Ras precipitated with anti-FLAG antibody. The activity compared to empty vector was represented as a bar graph. The experiments were repeated three times and error bar means S.D.

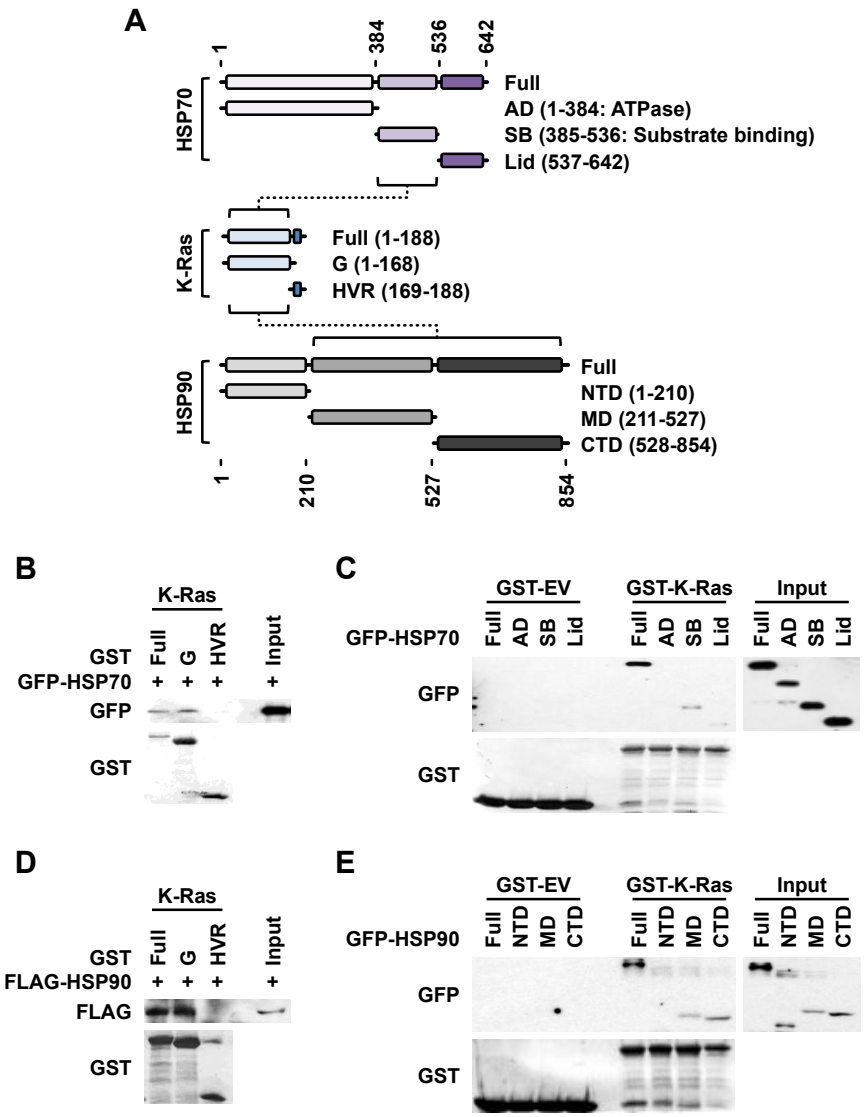

Figure 5. Determination of the domains involved in the interaction of K-Ras with HSP70 and HSP90

(A) This represents the arrangement of functional domains in HSP70, HSP90, and K-Ras. Each binding domains of the heat shock proteins and K-Ras marked with brackets and then connected with a dashed line.

(B) , (D) Each of the purified GST-K-Ras peptide containing full length, G domain and HVR was incubated with cell extracts containing GFP-HSP70 (B), and FLAG-SHP90 (D). GST proteins were precipitated with glutathione-sepharose beads, and co-precipitates were subjected to SDS-PAGE and immunoblotting using anti-GFP and anti–FLG antibodies for the determination of K-RAS-bound HSP70 and HSP90, respectively. GST proteins were measured by commassie staining.

(C), (E) Functional domains of GFP-tagged HSP70 (C) and HSP90 (E) were mixed with GST-K-Ras and the K-Ras-bound domains of HSP were determined as above.

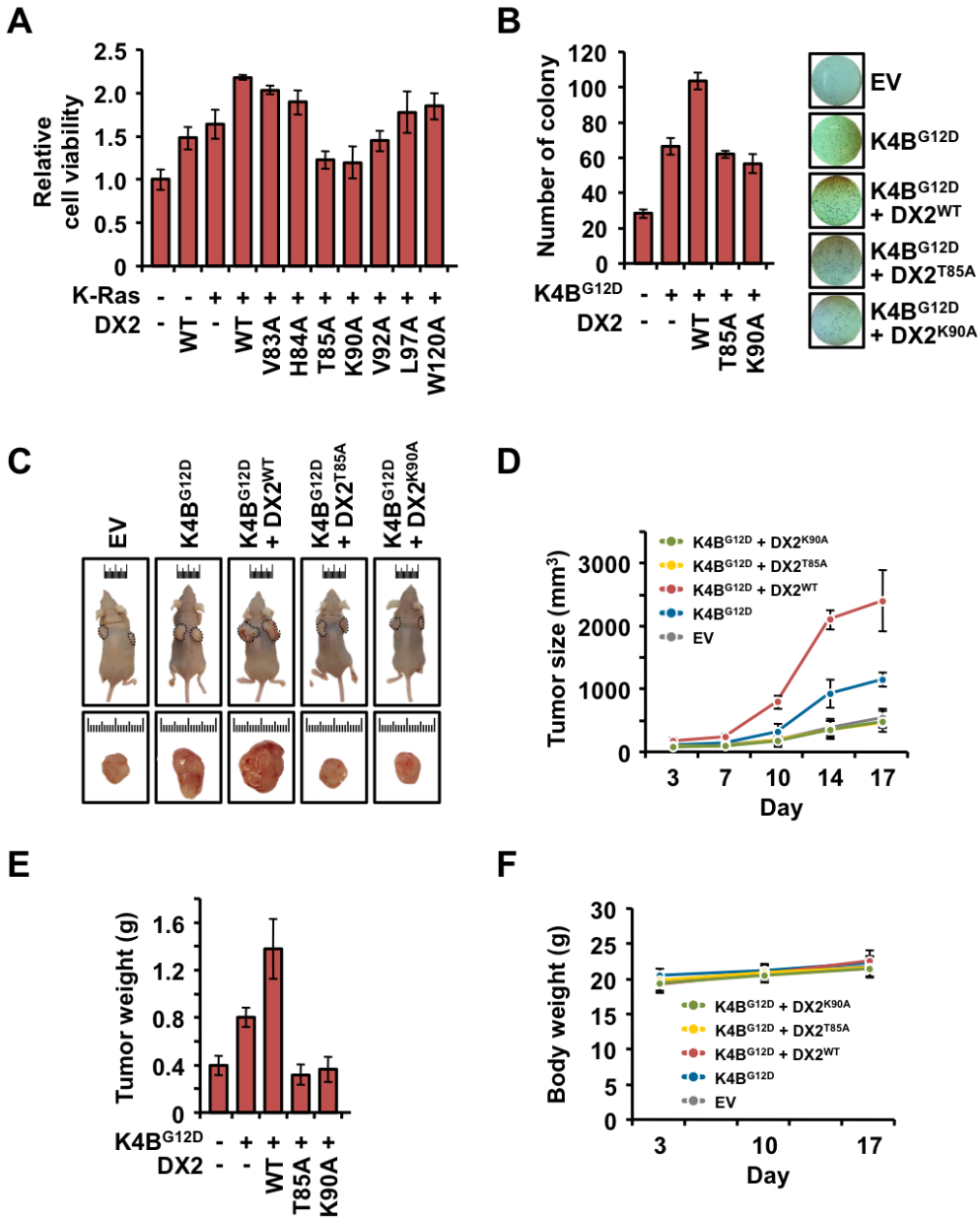
A
Relative cell viability
2.5
2.0
1.5
1.0
0.5
0
K-Ras - - + + + + + + + + +
DX2 - WT - WT V83A H84A T85A K90A V92A L97A W120A
B
Number of colony
120
100
80
60
40
20
0
K4B^G12D - + + + +
DX2 - - WT T85A K90A
EV
K4B^G12D
K4B^G12D + DX2^WT
K4B^G12D + DX2^T85A
K4B^G12D + DX2^K90A
C
EV
K4B^G12D
K4B^G12D + DX2^WT
K4B^G12D + DX2^T85A
K4B^G12D + DX2^K90A
D
Tumor size (mm^3)
3000
2000
1000
0
K4B^G12D + DX2^K90A
K4B^G12D + DX2^T85A
K4B^G12D + DX2^WT
K4B^G12D
EV
3 7 10 14 17
Day
E
Tumor weight (g)
1.6
1.2
0.8
0.4
0
K4B^G12D - + + + +
DX2 - - WT T85A K90A
F
Body weight (g)
30
25
20
15
10
5
0
K4B^G12D + DX2^K90A
K4B^G12D + DX2^T85A
K4B^G12D + DX2^WT
K4B^G12D
EV
3 10 17
Day

Figure 6. AIMP2-DX2 enhances the oncogenecity of K-Ras

(A) GFP-K-Ras and each of Strep-AIMP2-DX2 mutants were co-expressed in HCT-116 cells and the cell viability was determined by MTT assay.

(B) Strep-AIMP2-DX2 wild type (WT), T85A and K90A were introduced into K-Ras-expressed HCT116 cells. Each cell was subjected to anchorage-independent colony forming assay. The number of colony was counted and shown as a bar graph (Left). The image was shown (Right). The experiments were repeated three times and error bar means S.D.

(C) , (D) HCT-116 cells, stably expressing the indicated combinations of K-Ras4B^{G12D} with AIMP2-DX2 WT, T85A or K90A, were xenografted to nude mice and grown for 17 days. The time-dependent tumor growth was shown as a line graph (D) and representative images of the mice and tumors from each group were shown (C).

(E) Tumor weights were measured and shown as a bar graph.

(F) Body weights were measured three times and presented as a line graph.

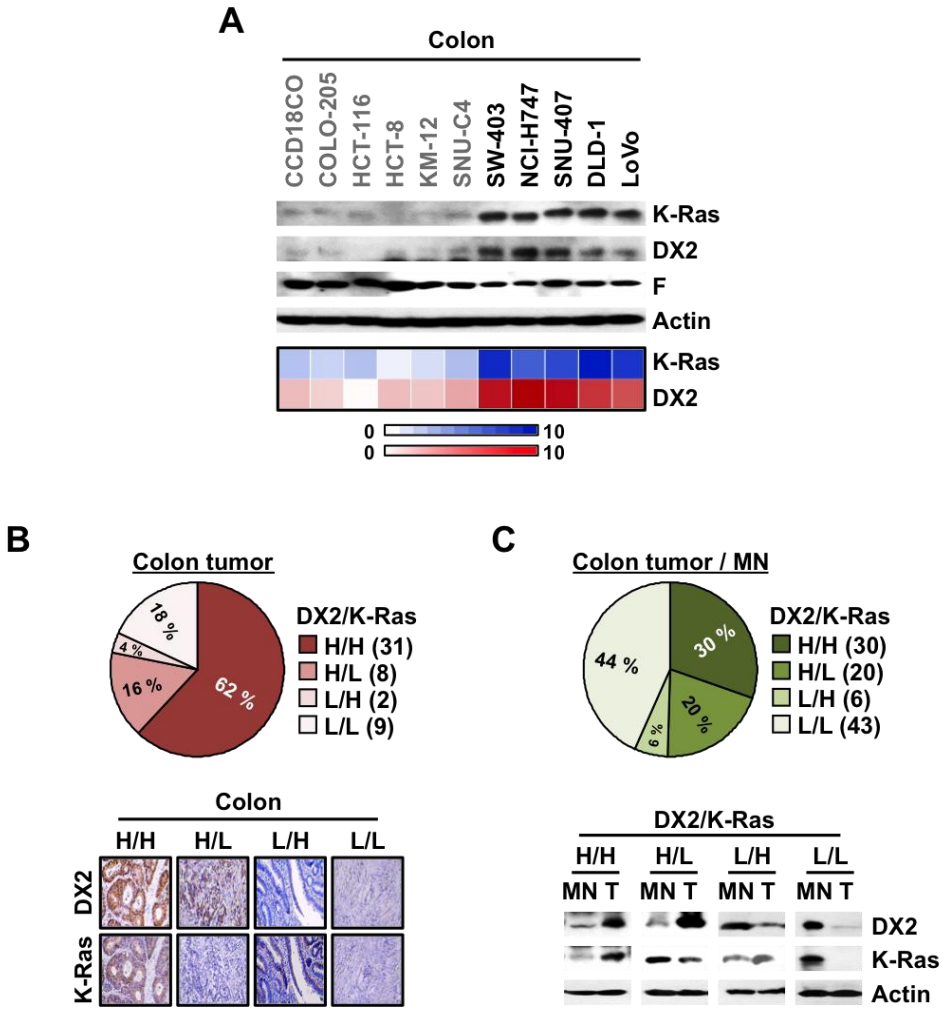

Figure 7. Positive correlation of AIMP2-DX2 and K-Ras levels in colon cancer

(A) Eleven colon cell lines, CCD18CO, COLO-205, HCT-116, HCT-8, KM-12, SNU-C4, SW-403, NCI-H747, SNU-407, DLD-1, and LoVo, were cultured. Then, the lysates from each cell lines were analyzed by Western blotting.

Levels of AIMP2-DX2 and K-Ras were normalized by actin level and represented as heat map.

(B) Tissue micro array (TMA) slides containing tumors from colorectal cancer patients were subjected to immunohistochemistry (IHC) staining with AIMP2-DX2 and K-Ras antibodies. After staining, the level of AIMP2-DX2 and K-Ras were analyzed.

(C) The levels of AIMP2-DX2 and K-Ras were analyzed by Western blotting using their specific antibody in tumor and matched normal (MN) tissues that were isolated from 99 colorectal cancer patients. Actin was used as a control. Depending on the levels in tumor compared to normal, the samples were classified as high and low.

Figure 8. Schematic Model

Un-stabilized –K-Ras interacts with AIMP2-DX2. Then, HSP70 and HSP90 are

recruited to the site where K-Ras and AIMP2-DX2 exsits. After that, K-Ras is properly folded by heat shock protein complex and the oncogeneity of K-Ras activated which results tumor progression.

DISCUSSION

In this study, I have clarified that AIMP2-DX2, oncogenic protein, as a key determinant that enhances the tumorigenisis of K-Ras by recruiting the heat shock protein complex. The GST domain of AIMP2-DX2 specifically binds to the C-terminal hypervariable region of K-Ras resulting the stability in protein level of K-Ras. This result was confirmed by creating K-Ras binding-defective AIMP2-DX2 mutants based on the NMR data. When K-Ras cannot interact with AIMP2-DX2, the expression level and the oncogenicity of K-Ras were reduced. Moreover, AIMP2-DX2 recruits HSP70 and HSP90 to fold K-Ras precisely. Based on the interactome analysis of K-Ras, heat shock protein complex, HSP70 and HSP90, were found as significant players to stabilize the K-Ras. And, it was possible to figure out each binding sites of AIMP2-DX2, K-Ras, and heat shock proteins when they bind each other using immunoprecipitation and pull down assay. It was clear that AIMP2-DX2 must be needed to turn on the activity of heat shock protein complex. However, the precise signal pathway and MOA how AIMP2-DX2 recruits HSP70 and HSP90 still need to be solved. Yet, the interaction of AIMP2-DX2 and K-Ras increased cell proliferation *in vitro* condition and tumor growth *in vivo* setting. Also, a strong positive correlation between the level of AIMP2-DX2 and K-Ras were observed in human colon cancer cell lines and in CRC patient tissues.

Based on the results from this study, down-regulation of AIMP2-DX2 via targeting has two merits. First, it is possible to regulate the level of K-Ras directly. Most of marketed drugs or therapeutics have limitation; they regulate the K-Ras

indirect way. However, I have checked that control the expression level of AIMP2-DX2 directly regulates the expression level of K-Ras. Therefore, decrease the level of AIMP2-DX2 results the decline the level of oncogenic protein of K-Ras. Second, AIMP2-DX2 blocks the tumor suppressor activity of AIMP2-F in various signals. Therefore, decline of AIMP2-DX2 will lead to the enhanced tumor suppressor activity of AIMP2-F, resulting in regression of cancer.

This study suggests that AIMP2-DX2 is a novel target to regulate the K-Ras. Moreover, inhibition of interaction between AIMP2-DX2 and K-Ras can be a new approach toward drug development on targeting K-Ras. Targeting AIMP2-DX2 will be a novel and effective treatment for major cancers without good drugs.

Reference

1 Hancock, J. F. Ras proteins: different signals from different locations. *Nat Rev Mol Cell Biol* **4**, 373-384 (2003).

2 Wennerberg, K., Rossman, K. L. & Der, C. J. The Ras superfamily at a glance. *J Cell Sci* **118**, 843-846 (2005).

3 Pylayeva-Gupta, Y., Grabocka, E. & Bar-Sagi, D. RAS oncogenes: weaving a tumorigenic web. *Nat Rev Cancer* **11**, 761-774 (2011).

4 Choi, J. W. *et al.* Cancer-associated splicing variant of tumor suppressor AIMP2/p38: pathological implication in tumorigenesis. *PLoS Genet* **7**, e1001351 (2011).

5 Oh, A. Y. *et al.* Inhibiting DX2-p14/ARF Interaction Exerts Antitumor Effects in Lung Cancer and Delays Tumor Progression. *Cancer Res* **76**, 4791-4804 (2016).

6 Prior, I. A., Lewis, P. D. & Mattos, C. A comprehensive survey of Ras mutations in cancer. *Cancer Res* **72**, 2457-2467 (2012).

7 Sunaga, N. *et al.* Knockdown of oncogenic KRAS in non-small cell lung cancers suppresses tumor growth and sensitizes tumor cells to targeted therapy. *Mol Cancer Ther* **10**, 336-346 (2011).

8 Ardito, C. M. *et al.* EGF Receptor Is Required for KRAS-Induced Pancreatic Tumorigenesis. *Cancer Cell* **22**, 304-317 (2012).

9 Avraham, R. & Yarden, Y. Feedback regulation of EGFR signalling: decision making by early and delayed loops. *Nat Rev Mol Cell Biol* **12**, 104-

117 (2011).

10 Bos, J. L., Rehmann, H. & Wittinghofer, A. GEFs and GAPs: critical elements in the control of small G proteins. *Cell* **129**, 865-877 (2007).

11 Stephen, A. G., Esposito, D., Bagni, R. K. & McCormick, F. Dragging ras back in the ring. *Cancer Cell* **25**, 272-281 (2014).

12 Bollag, G. & Zhang, C. Drug discovery: Pocket of opportunity. *Nature* **503**, 475-476 (2013).

13 Cox, A. D., Fesik, S. W., Kimmelman, A. C., Luo, J. & Der, C. J. Drugging the undruggable RAS: Mission possible? *Nat Rev Drug Discov* **13**, 828-851 (2014).

14 Spiegel, J., Cromm, P. M., Zimmermann, G., Grossmann, T. N. & Waldmann, H. Small-molecule modulation of Ras signaling. *Nat Chem Biol* **10**, 613-622 (2014).

15 Walther, A. *et al.* Genetic prognostic and predictive markers in colorectal cancer. *Nat Rev Cancer* **9**, 489-499 (2009).

16 Han, J. M. *et al.* Hierarchical network between the components of the multi-tRNA synthetase complex: Implications for complex formation. *J Biol Chem* **281**, 38663-38667 (2006).

17 Cho, H. Y. *et al.* Assembly of Multi-tRNA Synthetase Complex via Heterotetrameric Glutathione Transferase-homology Domains. *J Biol Chem* **290**, 29313-29328 (2015).

18 Kim, D. G. *et al.* Oncogenic Mutation of AIMP2/p38 Inhibits Its Tumor-Suppressive Interaction with Smurf2. *Cancer Res* **76**, 3422-3436 (2016).

19 Ahearn, I. M., Haigis, K., Bar-Sagi, D. & Philips, M. R. Regulating the regulator: post-translational modification of RAS. *Nat Rev Mol Cell Biol* **13**, 39-51 (2011).

20 Jha, R. *et al.* Purification and biophysical characterization of the AIMP2-DX2 protein. *Protein Expr Purif* **132**, 131-137 (2017).

21 Han, J. M. *et al.* AIMP2/p38, the scaffold for the multi-tRNA synthetase complex, responds to genotoxic stresses via p53. *Proc Natl Acad Sci U S A* **105**, 11206-11211 (2008).

22 Huntley, R. P. *et al.* The GOA database: gene Ontology annotation updates for 2015. *Nucleic Acids Res* **43**, D1057-1063 (2015).

23 Taipale, M., Jarosz, D. F. & Lindquist, S. HSP90 at the hub of protein homeostasis: emerging mechanistic insights. *Nat Rev Mol Cell Bio* **11**, 515-528 (2010).

24 Alvira, S. *et al.* Structural characterization of the substrate transfer mechanism in Hsp70/Hsp90 folding machinery mediated by Hop. *Nat Commun* **5**, 5484 (2014).

25 Birkeland, E. *et al.* KRAS gene amplification and overexpression but not mutation associates with aggressive and metastatic endometrial cancer. *Br J Cancer* **107**, 1997-2004 (2012).

26 Valtorta, E. *et al.* KRAS gene amplification in colorectal cancer and impact

on response to EGFR-targeted therapy. *Int J Cancer* **133**, 1259-1265 (2013).

27 Taya, Y. *et al.* A novel combination of K-ras and myc amplification accompanied by point mutational activation of K-ras in a human lung cancer. *EMBO J* **3**, 2943-2946 (1984).

28 Almoguera, C. *et al.* Most Human Carcinomas of the Exocrine Pancreas Contain Mutant C-K-Ras Genes. *Cell* **53**, 549-554 (1988).

29 Koo, K. H. *et al.* K-Ras stabilization by estrogen via PKCdelta is involved in endometrial tumorigenesis. *Oncotarget* **6**, 21328-21340 (2015).

30 Jeong, W. J. *et al.* Ras Stabilization Through Aberrant Activation of Wnt/beta-Catenin Signaling Promotes Intestinal Tumorigenesis. *Science Signaling* **5**, ra30 (2012).

국문초록

발암성 변이체인 AIMP가 Heat Shock Protein Complex을 매개체로 이용하여 K-Ras를 안정화시켜 대장암을 유발하는 과정에 대한 규명

서울대학교
융합과학기술대학원
분자의학 및 바이오제약학과 의약생명과학전공
노윤아

대장암은 세계적으로 꾸준히 증가하고 있는 암이다. 대장암 환자에게 처방되는 약은 부작용을 일으킬 뿐만 아니라 EGFR의 변이, 내성을 유발하기 때문에 보다 근본적인 치료법이 요구 되고 있다. 지금까지 밝혀진 연구에 따르면 대장암을 유발하는 가장 큰 원인은 K-Ras 단백질의 변형 때문이라고 알려져 있기 때문에 돌연변이 K-Ras를 억제하여 대장암을 치료하려는 시도가 있었다. 하지만, 어떻게 K-Ras가 돌연변이가 되어 암을 유발시키는 과정에 대해 자세히 알려진 바가 없기 때문에 난제로 남아있었다. 본 연구에서는 AIMP2-DX2가 K-Ras의 종양형성 능력을 Heat shock protein complex를 매개체로 하여 강화시키는 것을 확인하였다.

본래 AIMP2 (Aminoacyl-tRNA Synthetase complex-interacting multifunctional protein 2)는 아미노아실-티알엔에이 합성효소 (aminoacyl tRNA synthetase)를 포함하는 복합체의 형성에 관련 된 물질이자 여러 신호전달 하에서 암 억제제로 작용하는 단백질이다. 하지만, 엑손(exon) 2가 결손된 AIMP2-DX2는 야생형 AIMP2의 돌연변이이며, 암을 촉진시키는 단백질이다. AIMP2-DX2가 K-Ras에만 선택적으로 결합하여, K-Ras의 대장 종양 형성 능력을 촉진시키는 것을 확인하였다. 이 과정에서 AIMP2-DX2는 HSP70과 HSP90에게 K-Ras를 전달하여 K-Ras 단백질 구조를 더욱 안정화시키는 것 또한 확인하였다. AIMP2-DX2 와 K-Ras 의 상관관계와 암을 유발하는 정도를 시험관 내 (in vitro) 실험 및 생체 내 (in vivo) 실험을 통해 증명하였을 뿐만 아니라, 대장암 환자들의 암조직과 정상조직의 비교를 통해 밝혔다.

결론적으로 본 연구를 통해 AIMP2-DX2가 K-Ras만을 선택적으로 조절하는 중요한 조절인자임을 밝혔으며, 대장암 치료를 가능하게 할 우수한 표적인자임을 제시하였다.

주요어 : AIMP2-DX2, K-Ras, Hsp70, Hsp90, Heat Shock Protein Complex, 대장암, 종양, 병리학, 치료적암시

학 번 : 2016-26007